Chemistry Faculty Research & Creative Works   Chemistry

01 Jan 2023

Topology Driven And Soft Phonon Mode Enabled Na-ion Diffusion In Quaternary Chalcogenides, Na3ZnGaX4 (X = S, And Se)

Sajan Kumar

Mayanak K. Gupta

Ranjan Mittal

Santhoshkumar Sundaramoorthy

et. al. For a complete list of authors, see https://scholarsmine.mst.edu/chem_facwork/3653

Topology driven and soft phonon mode enabled Na-ion diffusion in quaternary chalcogenides, Na₃ZnGaX₄ (X = S, and Se)†

Sajan Kumar,[ab] Mayanak K. Gupta, [ID] *[ab] Ranjan Mittal, [ID] *[ab]
Santhoshkumar Sundaramoorthy, [ID] [c] Amitava Choudhury, [ID] *[c] Naresh C. Osti, [ID] [d]
Alexander I. Kolesnikov, [ID] [d] Matthew B. Stone, [ID] [d] Yongqiang Cheng[d]
and Samrath L. Chaplot [ID] [ab]

The compounds Na₃ZnGaX₄ (X = S, Se) are potential solid electrolyte materials in sodium-based batteries, which have certain advantages over oxide materials and have shown significant ionic conductivity at ambient temperature. In this paper, we bring out atomic-level features of the diffusion process in these new materials using the microscopic techniques of inelastic neutron scattering (INS), quasielastic neutron scattering (QENS), and *ab initio* molecular dynamics (AIMD) simulations. The insights obtained from these techniques are unique and not available from other macroscopic experiments. Neutron scattering experiments have been performed at temperatures from 100 to 700 K. The simulations have been carried out up to 900 K. We have calculated the phonon spectra and the space–time correlation functions and found good agreement with the results of the neutron scattering experiments. The simulations enable detailed analysis of the atomic-site dependent dynamical information. We observe low-energy phonon modes of ∼6 meV involving the vibrations of certain Na atoms in the lattice. This reveals that the Na at 32g Wyckoff sites (Na2) has sufficiently shallow potential among the two available crystallographic sites. This shallow potential facilitates diffusion. Furthermore, the specific structural topology of the network of interconnected zig-zag chains of the Na2 atomic sites provides the low-barrier energy pathways for diffusion. A small fraction of vacancy defects appears essential for diffusion. We further observe that the Na2 atoms undergo jump-like diffusion to the vacant next or the 2nd next neighbour sites at ∼4 Å. While the QENS experiments reveal the jump-like diffusion and its time scale, detailed analysis of the AIMD simulations shows that the jumps appear mostly along zig-zag chains of the Na2 sites in the tetragonal ab-plane, as well as between the chains along the c-axis. The net diffusion is essentially 3-dimensional, with little anisotropy despite the anisotropy of the tetragonal crystal structure.

1 Introduction

The demand for green energy has been increasing significantly in recent years to tackle the issue of global warming and climate change. Researchers are deeply involved in enhancing green energy or renewable energy production (solar energy, wind energy, hydro energy, and electro-chemical energy, *etc.*)[1–7] and better energy storage devices, *i.e.* batteries that are safer, with

longer duty cycles, higher energy density, higher power density, and more economically sustainable.[8–13] The present commercial batteries are primarily based on Li and use liquid- or gel elec-trolytes. They have several practical advantages, such as high ion conductivity and a wide electro-chemical window. On the other hand, they pose severe issues like the potential for catching fire, chemical instability, shorter useful lifespans, *etc*[14–17]. The limited abundance of Li-ion and its poor diversifi-cation has also raised serious concerns.[18–20] Sodium-ion batteries are considered the best alternative technology for future-generation energy storage systems.[21–27]

Some of the Na-based superionic conductors (Na₃.₃Zr₁.₈₅-Mg₀.₁₅Si₂PO₁₂, Na₁₊ₓ Zr₂ Siₓ P₃₋ₓ O₁₂ with x = 2–2.5, Na₃PS₄, Na₃OBH₄, and Na₁₁Sn₂PS₁₂) show greater potential as candi-dates for real-life applications due to high Na-ion conductivity, economic sustainability, thermally stable phase (in some cases), low thermal expansion coefficient, and rich abundance.[28–35] Despite having these advantages, they also suffer from poor

[a]Solid State Physics Division, Bhabha Atomic Research Centre, Mumbai, 400085, India. E-mail: mayankg@barc.gov.in; rmittal@barc.gov.in

[b]Homi Bhabha National Institute, Anushaktinagar, Mumbai 400094, India

[c]Department of Chemistry, Missouri University of Science and Technology, Rolla, MO 65409, USA. E-mail: choudhurya@mst.edu

[d]Neutron Scattering Division, Oak Ridge National Laboratory, Oak Ridge, Tennessee 37831, USA

interfacial contact between electrodes and electrolytes, often high ionic conductivity at elevated temperatures, and a high cation migration barrier energy at room temperature, which further limits their applicability.[7,36–38] To address these issues and further improve their applicability for common use, additional fundamental research is required. In this regard, it must be mentioned that some recently discovered Na-based superionic conductors containing chalcogenide elements like Na_3PS_4,[29,39] Na_3FCh (Ch = S, Se, and Te),[40,41] $Na_{11}Sn_2PS_{12}$,[31] Na_3SbS_4 (ref. 42–44) and Na_3ZnGaX_4 (X = S, Se)[45,46] are showing great promise with high ionic conductivity and low activation barriers at room temperature. Among these, Na_3ZnGaX_4 (X = S, Se) caught our attention because of their high air and aqueous stability and ability to further improve the ionic conductivity through compositional adjustments.[45] For example, Balijapelly *et al.* reported the ionic conductivity of 3.74×10^{-4} and 0.12 mS cm^{-1} at 303 K with activation barriers (E_b) of 0.42 and 0.38 eV, respectively, for Na_3ZnGaS_4 and $Na_3ZnGaSe_4$.[45] Alternatively, by increasing the amount of Ga and controlling the Na vacancy, Han *et al.* decreased the activation energy ($E_b = 0.30$ eV) and substantially increased the ionic conductivity (0.32 mS cm^{-1}) in $Na_{3-x}Zn_{1-x}Ga_{1+x}S_4$.[46] Balijapelly *et al.* reported that both compounds are moisture stable, i. e., not very sensitive to air. Following Balijapelly's work, Han *et al.* also demonstrated these compounds' excellent moisture and aqueous stability.[46] Therefore, we wanted to investigate these two pristine compounds, Na_3ZnGaX_4 (X = S, Se),[45,46] and delve much deeper into the microscopic origin of good ionic conductivity through a combination of neutron scattering experiments and molecular dynamic simulations. To understand the diffusion process of Na-ions at the microscopic level, we performed inelastic neutron scattering (INS) and quasielastic neutron scattering (QENS) experiments and *ab initio* molecular dynamics (AIMD) simulations. The INS study of these compounds investigates the phonon modes, which may play a role in facilitating Na-ion diffusion. QENS analysis provides information about stochastic dynamics related to diffusive species. Our AIMD simulations supplement these measurements and further explore the microscopic details of the Na diffusion mechanism.

2 Experimental

The Na_3ZnGaX_4 (X = S, Se) chalcogenide compounds are prepared by solid–state reactions in a sealed quartz tube. The details of synthesis and characterisation are given in the ESI† (Fig. S1 and Table S1†). We measured the phonon density of states of Na_3ZnGaX_4 (X = S, Se) compounds using INS at 100 K, 300 K, 400 K, 500 K, and 700 K. Two incident neutron energies have been used (E_i = 26 meV and E_i = 82.9 meV) using the SEQUOIA time of flight spectrometer[47] at the Spallation Neutron Source (SNS) at Oak Ridge National Laboratory(ORNL), USA.

The measured spectra were transferred to the dynamical structure factor, $S(Q, E)$, and corrected for the background spectra of an empty quartz ampule in the aluminium container measured under similar conditions. Assuming the incoherent approximation (when the powder data are averaged over an extended Q range), the $S(Q, E)$ data were further transferred to

neutron-weighted phonon density of states $g^n(E)$ using the following relation.[48]

$$g^n(E) = A\left\langle \frac{e^{2W(Q,T)}}{Q^2} \frac{E}{n(E,\ T)+1} S(Q,\ E) \right\rangle \quad (1)$$

where A is the normalisation factor, $\langle \cdots \rangle$ denotes the averaging over Q (wave-vector transfer), $n(E,\ T)$ is the population of phonons at energy E and temperature T, which follows the Bose-Einstein distribution. $2W(Q,\ T)$ is the Debye-Waller factor, which was set to zero. We present data from the neutron energy loss side of the spectrum due to the better energy resolution in this range. The $g^n(E)$ were averaged over the Q range of 0.4 to 3 Å^{-1} for E_i = 26.0 meV while for E_i = 82.9 meV, $g^n(E)$ were averaged over the Q range of 0.5 to 5.2 Å^{-1}. We have corrected the measured data for a multiphonon contribution to the spectra, which is estimated from AIMD trajectories as described in the computational section.

The quasielastic neutron scattering (QENS) measurements of Na_3ZnGaX_4 (X = S, Se) at temperatures 100 K, 500 K, 600 K, and 700 K were carried out using the time-of-flight backscattering silicon spectrometer (BASIS)[49] at SNS at the ORNL, USA. An aluminium cylindrical sample holder with polycrystalline powder sample sealed in a quartz tube was used for the QENS measurements. The instrument energy resolution used for this set-up was 3.7 μeV. For these measurements, BASIS was operated to cover the Q range of 0.3 Å^{-1} to 1.9 Å^{-1} and the energy transfer range of ±100 μeV. The instrument energy resolution at this configuration was 3.7 μeV (Q-averaged full width at half maximum). QENS spectra were reduced using the Mantid software package.[50] The measured data convoluted with the sample specific resolution function (collected at 100 K) were fitted with one Lorentzian and one delta function.

3 Computation details

The lattice dynamics (LD) and AIMD simulations are based on the density functional theory, as implemented in the Vienna *Ab initio* Software Package (VASP).[51–53] The simulations used the projector-augmented wave (PAW) formalism[54] and the generalised gradient approximation (GGA) exchange-correlation functional parameterisation by Perdew, Burke, and Ernzerhof (PBE).[55,56]

3.1. Lattice dynamics

The phonon eigenvector calculation in 2% vacancy structure of Na_3ZnGaX_4 (X = S, Se) was performed on a $(\sqrt{2} \times \sqrt{2} \times 1)$ supercell (288 atom cell) of the tetragonal unit-cell using the finite displacement method implemented in the PHONOPY software.[57] A plane-wave energy cutoff of 600 eV was used. The convergence criteria for the electronic energy was set to 10^{-7} eV.

3.2. *Ab initio* molecular dynamics

The AIMD simulations were performed on a $(\sqrt{2} \times \sqrt{2} \times 1)$ supercell (288 atoms cell), and a plane-wave energy cutoff of 600 eV was used for AIMD simulations. However, the energy convergence criterion was set to 10^{-6} eV. AIMD simulation is

carried out using a single k-point at the zone centre. For these simulations, we used NVT ensembles where N is the number of particles, V is the volume, T is the temperature, and the Nose–Hoover thermostat[58] is used to maintain a constant temperature, T. We equilibrated the system for 10 ps, and the next 40–60 ps were used for production run using a time step of 2 fs. We performed AIMD simulation for two cases, namely, the stoichiometric and non-stoichiometric structures with 2% Na-vacancy labelled as 1 vac-NZGS and vac-NZGSe. The 2% Na-vacancy is created by randomly removing 2 Na atoms from 96 Na sites in the supercell. The details of the formalism for various thermodynamical and transport properties calculations are given in ESI.†(ref. 59)

4 Result and discussion

4.1. Brief description of structural features

The crystal structures of Na_3ZnGaX_4 (X = S, Se) have been described in the literature adequately.[45,46,60] Therefore, we briefly touch upon the salient structural features here. Both compounds are isostructural, crystallising in a tetragonal crystal system with space group $I4_1/acd$[60] (Fig. 1). They are quaternary chalcogenide compounds built up of T_2-type super-tetrahedron building units composed of four corner-shared ZnX_4/GaX_4 tetrahedral units. Such T_2 units are further corner-shared, forming a 3D network, and furthermore, two such 3D networks are interpenetrated. Two crystallographically distinct types of Na-ions are trapped in the channels formed by these interpenetrated lattices[45,60](Fig. 1). There are sixteen formula units per unit cell ($Z = 16$). The Na atoms occupy two types of positions, the 16f and 32g Wyckoff sites referred to as Na1 and Na2, respectively, and X (S/Se) atoms occupy three different

positions, the 32g, 16d, and 16e Wyckoff sites. The Ga and Zn occupy the 32g Wyckoff sites with 50% occupancy each.[45]

4.2. Inelastic neutron scattering and phonon density of states

The phonon density of states from the chalcogenide compounds Na_3ZnGaX_4 (X = S, Se) (i.e. NZGS and NZGSe, respectively) at various temperatures are shown in Fig. 2a and b. We performed INS measurements using $E_i = 26.0$ meV and $E_i = 82.9$ meV, providing good energy resolution in the low-E regime and capturing the complete phonon spectra of the system. The PDOS spectra show that the phonons extend up to 50 meV and 40 meV for NZGS and NZGSe, respectively. The low-E spectra obtained using $E_i \sim 26.0$ meV show a broad peak at $\sim$12 meV and $\sim$7 meV in NZGS and NZGSe, respectively. These peaks broaden significantly on warming and hence appear to be strongly anharmonic. We have calculated the partial and total PDOS using AIMD at various temperatures (Fig. S2a and S2b†)[59] to investigate the partial contribution of each atom to the total measured PDOS spectra. Furthermore, we also calculated the neutron-weighted partial PDOS of each species (Na, Ga, Zn, and X) from AIMD trajectories at 300 K (Fig. 2c and d)). From the neutron-weighted partial DOS calculation, the major contribution in the measured PDOS spectra below $\sim$25 meV seems to come from the Na- and Se-dynamics. We compared the experimental PDOS with the calculated neutron-weighted total PDOS for both compounds, and found that the AIMD calculated PDOS reasonably reproduces the experimental features (Fig. 2c and d). We also computed the band centre from total DOS and found that the phonon band centre of NZGSe appears lower than that of NZGS (Fig. S3a†).[59] By comparing the neutron-weighted PDOS of NZGS and NZGSe (Fig. S3a†),[59] we found that NZGSe shows a larger PDOS below 10 meV than NZGS due to a softer lattice of NZGSe than NZGS.

To investigate the nature of vibrations and their role in Na diffusion, we computed the Wyckoff site-wise partial PDOS of Na in both compounds (Fig. 2e and f). Na at the 32g site shows a much broader phonon distribution with significant PDOS at lower energies than Na at the 16f site. The Na-diffusion may be guided by the low-E phonon modes involving the large amplitude of vibrations of the Na2 (32g). We also looked into the eigenvectors of the low-E modes ($\sim$ 5.8 meV) and drew a representative mode in Fig. 3a and b. We observed that the Na at 32g Wyckoff sites shows significantly larger displacement than at 16f Wyckoff sites. This displacement is also evident from the calculated contribution of phonon of energy E to MSD at 900 K (Fig. 3c and d). We anticipate that the shallower potential energy surface at 32g Wyckoff sites leads to a larger MSD than at 16f Wyckoff sites. As discussed in the next section, diffusion is dominated through the Na2 sites.

4.3. Quasi-elastic neutron scattering

We have performed the temperature-dependent QENS measurements on Na_3ZnGaX_4 (X = S, Se) at 100 K, 500 K, 600 K, and 700 K (Fig. 4a and b). Note that the broadening of the QENS signal reveals the stochastic dynamics in a system. A noticeable
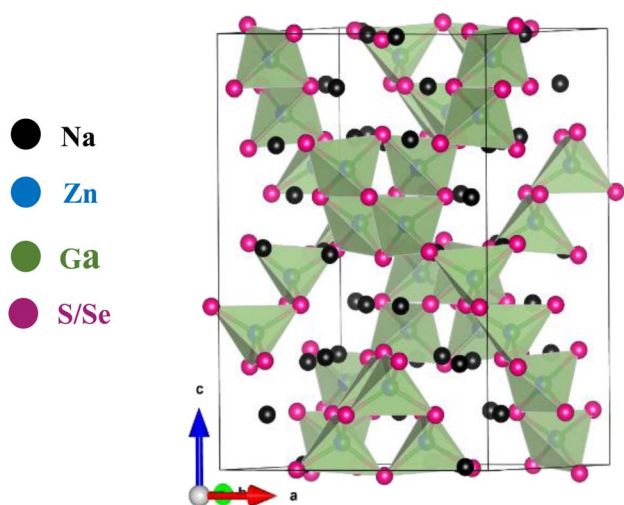

Fig. 1 The tetragonal crystal structure of Na_3ZnGaX_4 (body-centred tetragonal, space group $I4_1/acd$, $Z = 16$), where (X = S, Se). Zn and Ga occupy 32g Wyckoff sites with occupancies 0.5 : 0.5 and form the polyhedral unit Zn/GaX$_4$. The room temperature lattice parameters of Na_3ZnGaX_4 (X = S/Se) are $a = b = 12.925/13.43$ Å and $c = 18.623/19.15$ Å.

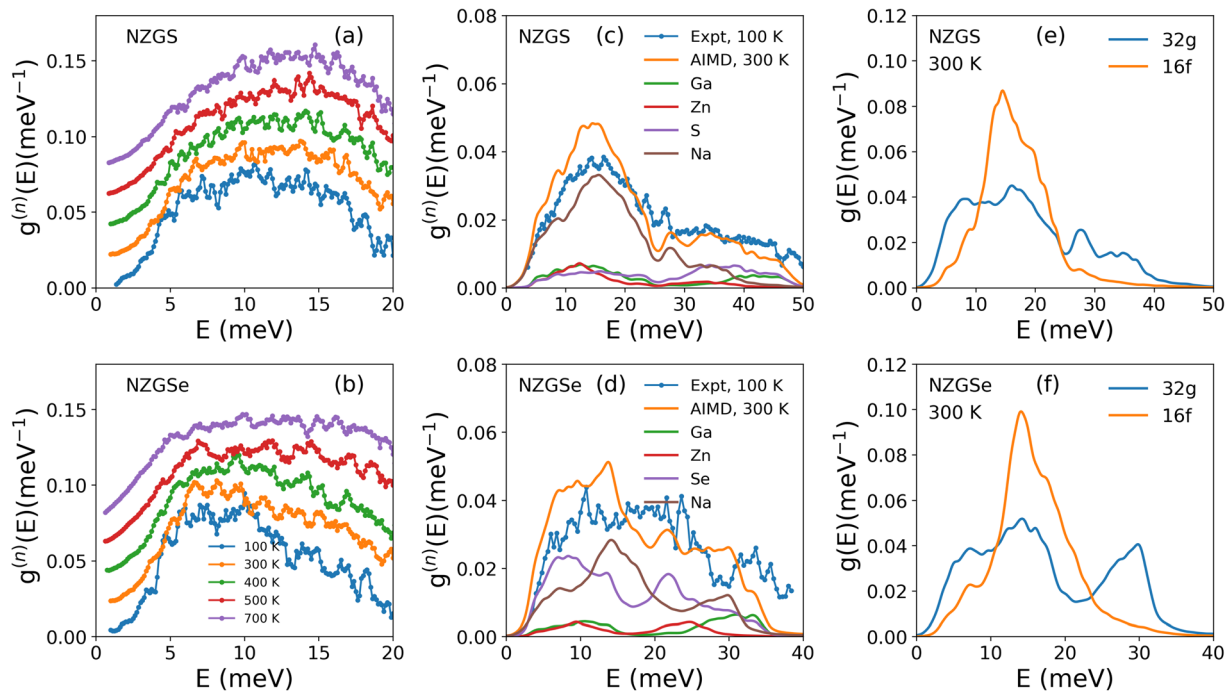**Fig. 2** (a and b) The measured temperature dependence of neutron-weighted PDOS of Na_3ZnGaX_4 (X = S, Se) compound using 26.0 meV incident neutron energy. (c and d) The calculated partial contribution of various species in Na_3ZnGaX_4 (X = S, Se) to total neutron weighted PDOS and compared with 100 K measured PDOS using 82.9 meV incident neutron energy. (e and f) The calculated partial phonon density of states of Na atoms at $32g$ and $16f$ Wyckoff sites.

QENS broadening is observed at 700 K, indicating the presence of diffusion at 700 K (Fig. 4a and b). The measured S(Q, E) is analysed using a single Lorentzian function convoluted with the instrumental resolution function. A linear background term is also added to account for the faster motion that falls outside of the instrument energy coverage window.[59] The relative spectral weight of the quasielastic area ($A_{Lorentzian}$) with respect to the elastic component ($A_{Elastic}$) as a function of Q is given in Fig.-S3e.†(ref. 59) We have extracted the QENS width, Γ, from the measured spectra within a Q range of 0.2 < Q < 1.1 Å^{-1} in both the compounds at 700 K. In Fig. 4c and d, we have shown the Q dependence of Γ fitted with the Chudely-Elliot (CE) model,[61] a jump-diffusion model, as given below,

$$\Gamma(Q) = \frac{\hbar}{\tau}\left(1 - \frac{\sin(Qd)}{Qd}\right) \qquad (2)$$

where, $\Gamma(Q)$ is the half width at half maximum (HWHM) of a Lorentzian at wavevector transfer Q, d and τ are the jump-length and mean residence time of the diffusing atoms, respectively. Due to the limited Q-range of the QENS measurements, the simultaneous estimate of d and τ from the fitting of the CE-model was challenging. The diffusion coefficient is given by

$$D = d^2/6\tau \qquad (3)$$

Hence, we have estimated the d (for NZGS ∼3.75 Å while for NZGSe 3.83 Å) from the AIMD computed Na–Na Van–Hove

correlation function at 50 ps and fixed it while fitting the CE model to the QENS width. The estimated mean residence time from CE-model is ∼48 ps and ∼34 ps for NZGS and NZGSe, respectively. The QENS estimated diffusion coefficient at 700 K, using eqn (3), is 4.9×10^{-10} m^2 s^{-1} and 7.2×10^{-10} m^2 s^{-1} for NZGS and NZGSe, respectively. Notably, the QENS measurements show the same order of diffusion coefficient for both compounds, which agrees with the AIMD inferences discussed in the next section. We have also analysed the QENS data using the CE-model without imposing any constraints on jump-length and estimated the diffusion coefficients (Fig. S3d†).[59] The estimated diffusion coefficients with and without the constraints on the jump lengths are found to be similar within 15%.

We also calculated the dynamical structure factor S(Q, E) in vac-NZGS and vac-NZGSe for Q values up to 1.6 Å^{-1} at 900 K using the AIMD (Fig. S4 and S5†).[59] The estimated Lorentzian width (HWHM) is plotted with Q and fitted with the CE-model (Fig. 4e and f). We have used the above noted jump lengths estimated using the Van–Hove correlation function. The calculated diffusion coefficient from the CE-model is 6.3×10^{-10} m^2 s^{-1} and 5.5×10^{-10} m^2 s^{-1} for NZGS and NZGSe, respectively, showing the same order of diffusion coefficient as obtained from the QENS data.

4.4. Na$^+$ ion diffusion, hopping mechanism, and Van–Hove correlation functions

In the QENS section, we showed a significant quasielastic broadening at elevated temperatures compared to room
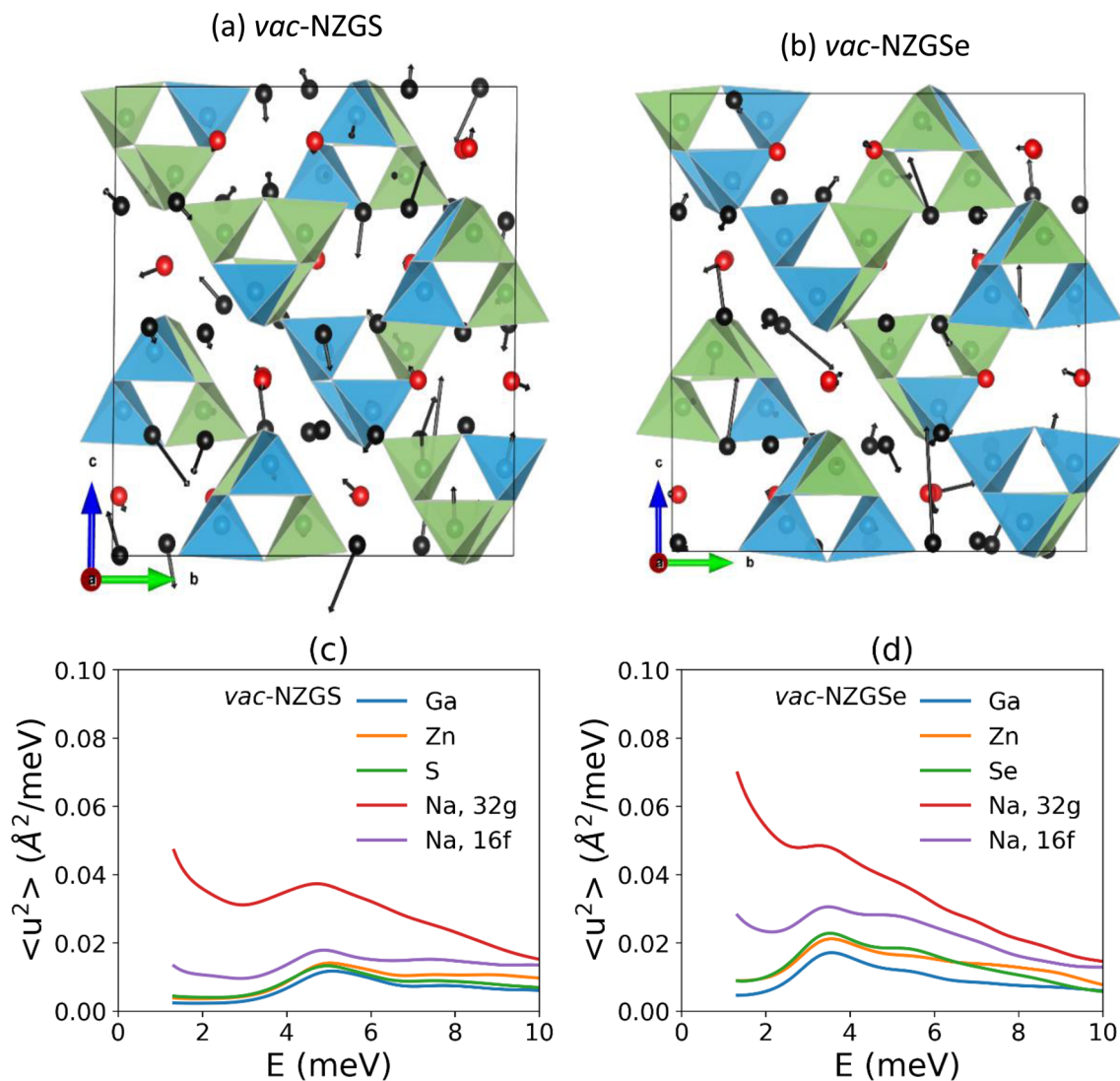
(a) *vac*-NZGS

(b) *vac*-NZGSe

(c)

(d)

Fig. 3 (a and b) The calculated harmonic phonon eigenvectors of 32g and 16f Wyckoff sites Na atoms in the vacancy structure of Na$_3$ZnGaX$_4$ (X = S, Se). The Na at 32g sites is indicated by black spheres, while at 16f sites is shown by red spheres. The displacements pattern for S and Se compounds are shown for phonon modes of energy 5.8 meV. We have shown only half of the unit cell boundary along the a-axis for clarity. The ZnX$_4$ and GaX$_4$ polyhedral units are indicated by green and blue colors, respectively. (c and d) The calculated energy dependence of averaged phonon contribution to MSD at 900 K of Na$_3$ZnGaX$_4$ (X = S, Se).

temperature. This broadening corresponds to stochastic dynamics, which invokes us to do further analysis. In the stoichiometric Na$_3$ZnGaX$_4$ (X = S, Se) (*n*-NZGS, *n*-NZGSe) materials, we calculated the MSD of individual species (Na$^+$, Ga^{3+}, Zn^{2+}, S^{2-}, Se^{2-}) at the different temperatures as shown in Fig. S6a and b.†(ref. 59) All the species showed time-independent MSD in stoichiometric Na$_3$ZnGaX$_4$ (X = S, Se), which clarifies that all atoms are localised around their respective equilibrium positions, possibly due to the non-availability of hopping sites. The MSD calculation with a 2% Na vacancy structure of Na$_3$ZnGaX$_4$ (X = S, Se) at different temperatures (Fig. 5a, b and S7a, b†)[59] shows an increasing behaviour with time, suggesting that only Na$^+$ are the diffusing ions. MSD of the rest of the species (Ga^{3+}, Zn^{2+}, S^{2-}, Se^{2-}) shows a time-independent plateau indicating that they are vibrating about equilibrium positions. Hence the

2% sodium deficient structure provides the necessary path for Na$^+$ to hop from one site to another site.

As discussed above, the phonon DOS of Na atoms at 32g and 16f Wyckof sites show a very different spectrum, indicating a significant difference in Na-host lattice interaction at 32g and 16f sites. To probe their impact on diffusion, we have computed the Wyckoff site resolved Na-MSD. In Fig. 5c and d), we showed the Wyckoff site-specific MSD for both chalcogenide compounds (*vac*-NZGS and *vac*-NZGSe). We found that the MSD of Na atoms at 32g sites has a large contribution to the total MSD, while the MSD of Na atoms at 16f sites has the least impact. To get better insights into the hopping mechanism of each Na atom at 32g sites and 16f sites, we calculated the MSD of individual Na atoms up to 30 ps and 60 ps at 900 K in both compounds.[59] Many Na atoms at 32g sites show hops with
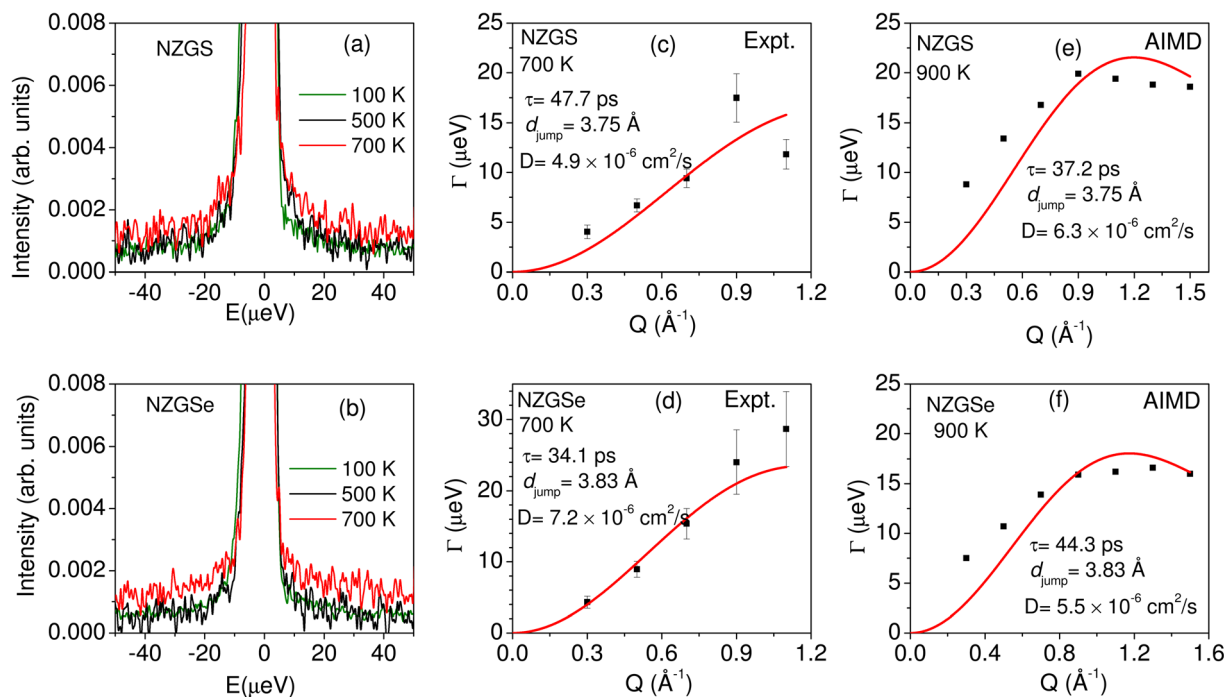
Fig. 4 (a and b) The measured $S(Q, E)$ of Na_3ZnGaX_4 (X = S, Se) compound at various temperatures using QENS. (c and d) The estimated half width at half maximum (HWHM) at Q regime (<1.2 Å^{-1}) of Na_3ZnGaX_4 (X = S, Se) compound using Lorentzian fitting of $S(Q, E)$ at 700 K, analysed with C-E model (red solid line). (e and f) The calculated HWHM from simulated $S(Q, E)$ using AIMD trajectories in *vac*-NZGS and *vac*-NZGSe, analysed with the C-E model (red solid line).

a jump length of ~4 Å, while very few Na atoms at 16*f* sites show any jumps, which signifies that Na atoms at 32*g* sites are more diffusive than 16*f* sites. The diffusion coefficient from AIMD simulations shows similar behaviour to that of the experiment, which further validates the approach that we have employed for the QENS data analysis.
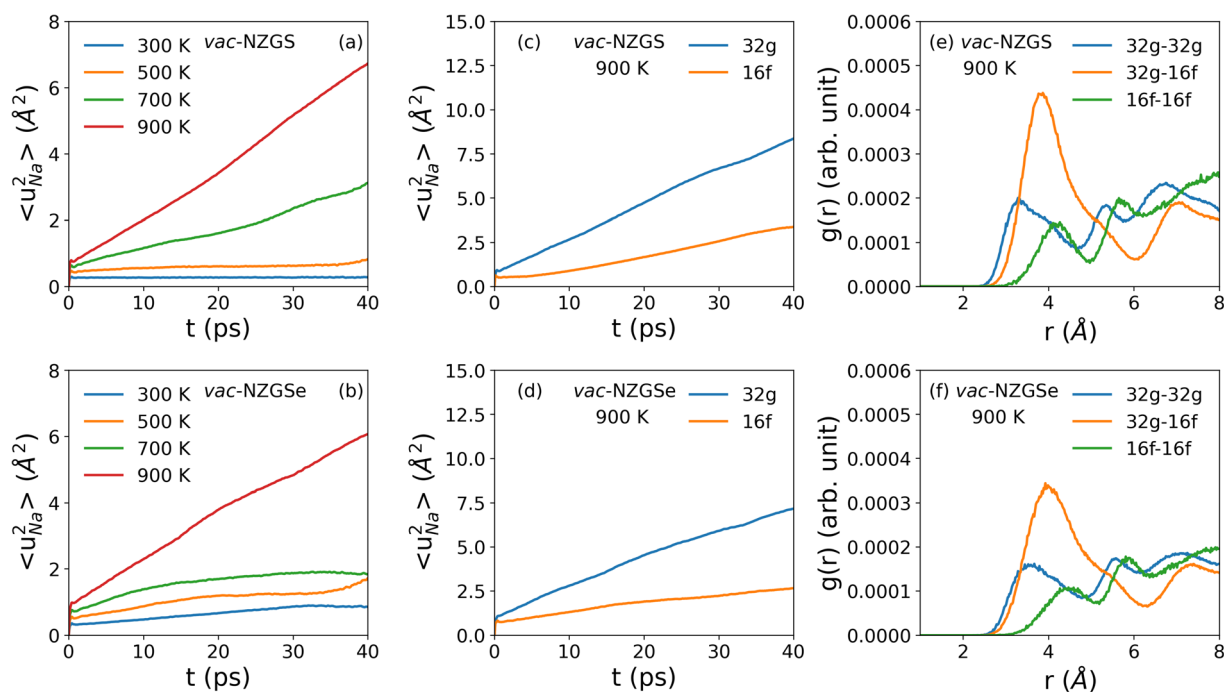

Fig. 5 (a and b) The calculated Na-MSD with 2% Na vacancy in Na_3ZnGaX_4 (X = S, and Se) at various temperatures using AIMD trajectories. (c and d) The calculated site specific Na-MSD between 32*g*–32*g* and 16*f*–16*f* Wyckoff sites in *vac*-NZGS and *vac*-NZGSe. (e and f) The calculated Na–Na PDF between Na at 16*f* and 32*g* Wyckoff sites of *vac*-NZGS and *vac*-NZGSe.
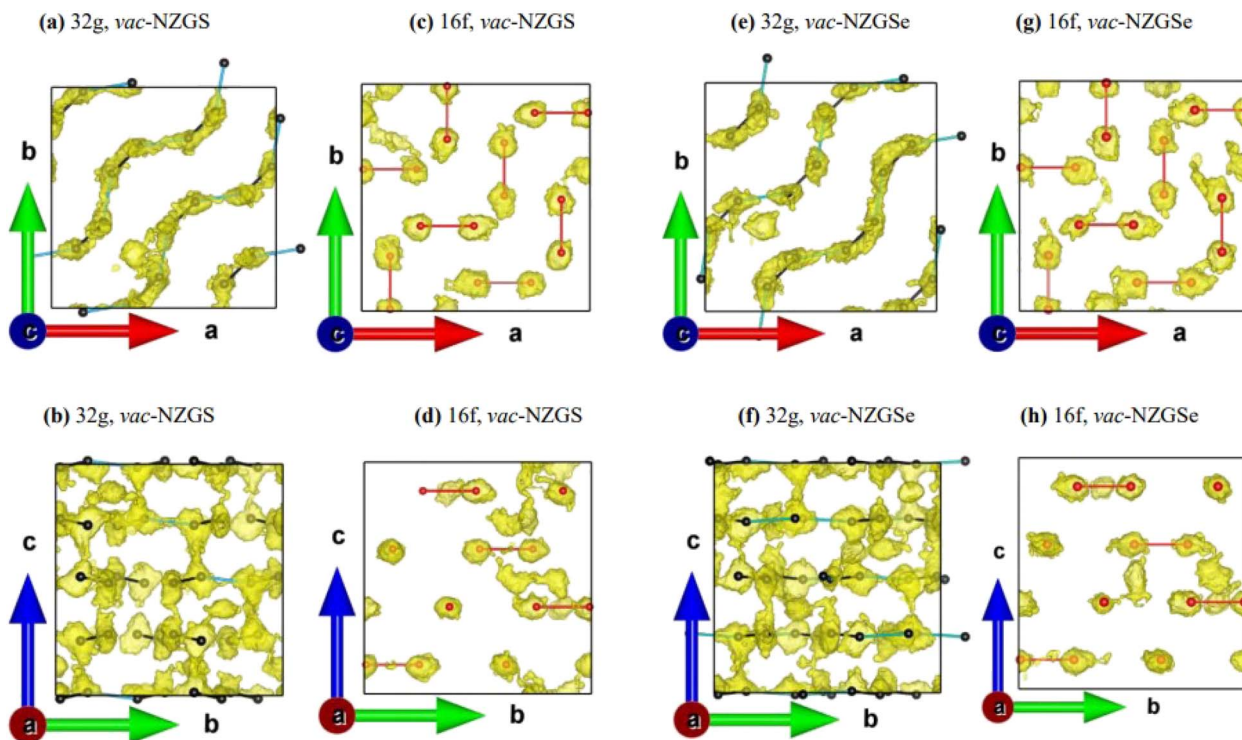
Fig. 6 The Na-Occupation probability-density (isosurface value $\sim 0.001/\text{Å}^3$) of Na^+ initially occupied 16f and 32g Wyckoff sites, calculated using AIMD trajectories of vac-NZGS. (a–d) vac-NZGS, and (e–h) vac-NZGSe at 900 K. The Na at 32g sites are shown as black spheres, while the 16f sites are indicated by red spheres. The black and light blue bonds represent the first and second neighbour distances between Na's occupied at 32g sites. The first/second neighbour distances for Na at 32g sites are 3.2 Å/4.06 Å and 3.36 Å/4.17 Å, for NZGS and NaZGSe, respectively. The red bonds represent the first neighbour distance between Na's occupied at 16f sites. The first neighbour distances between Na at 16f sites are 4.25 Å and 4.47 for NZGS and NaZGSe, respectively. Differences between the panels are described in the main text.

To map the Na^+ diffusion pathways, we calculated the Na-occupation probability density in vacancy structure (vac-NZGS, vac-NZGSe) at 900 K using AIMD. The Na-probability isosurface plot (Fig. 6 and Fig. S9a and b†)[59] shows connectivity from one Na-site to another Na-site in both compounds, indicating possible paths of Na^+ diffusion. For precise observations, we calculated Wyckoff site-specific Na occupation probability (Fig. 6a–h) for Na atoms at 32g and 16f sites in the ab- and bc-plane for both compounds (vac-NZGS and vac-NZGSe). This calculation shows that the Na atoms at 32g Wyckoff sites are well connected and provide long-range diffusion pathways. However, Na at 16f sites shows disconnected localised density, indicating the negligible Na conductivity contributed from Na at 16f sites. These plots show that the Na2 (32g Wyckoff) sites are connected along zig-zag chains in the ab-plane, indicating jumps through these sites along the chains. These chains are almost planar in the ab-plane with a small buckling of $\sim$0.4 Å, and they are separated by $\sim$c/4 along the c-axis. We also observe jumps between the Na2 sites on one chain to another along the c-axis. The larger MSD for Na atoms at 32g sites in comparison to 16f may be due to the fact that the atoms at 32g have a specific structural topology of the network of interconnected zig-zag chains, which provides the low-barrier energy pathways for diffusion. As discussed above, diffusion of the Na atoms at the 32g site is enabled by a relatively shallow potential of the low-energy phonons.

The Na migration energy barrier (E_b) is estimated from the probability density using the following relations,[41]

$$E_b = -k_B T \ln\left(\frac{\rho_{th}}{\rho_{max}}\right) \qquad (4)$$

where K_B is the Boltzmann constant, T is the temperature, ρ_{th} is the threshold isosurface value at which the Na-sites are just connected and ρ_{max} is the maximum isosurface value. The estimated migration barrier energy for the vac-NZGS compound is $\sim$ 0.30 eV, and for vac-NZGSe, it is $\sim$ 0.27 eV, which is comparable to the reported values from the conductivity measurements.

To visualise the possible pathways of Na^+ hopping in both 2% Na-deficient chalcogenide compounds (vac-NZGS and vac-NZGSe), we calculated the trajectory of randomly chosen Na^+ up to 60 ps with 120 fs time step at 900 K shown in Fig. S9c and d.†(ref. 59) Na^+ dwells a few picoseconds at present sites before jumping to neighbour Na-sites, which lie at a distance of $\sim$ 4 Å. The calculated Na trajectory up to 60 ps shows direction-independent long-range diffusion. We have also shown the trajectory of the Na atom for n-NZGS and n-NZGSe in Fig. S9e and f.†(ref. 59)

To further investigate the hopping mechanism in both chalcogenide compounds (vac-NZGS and vac-NZGSe), we calculated the self Van–Hove correlation function up to 20 ps with 4 ps time frame for n-NZGS and n-NZGSe at 700 K using
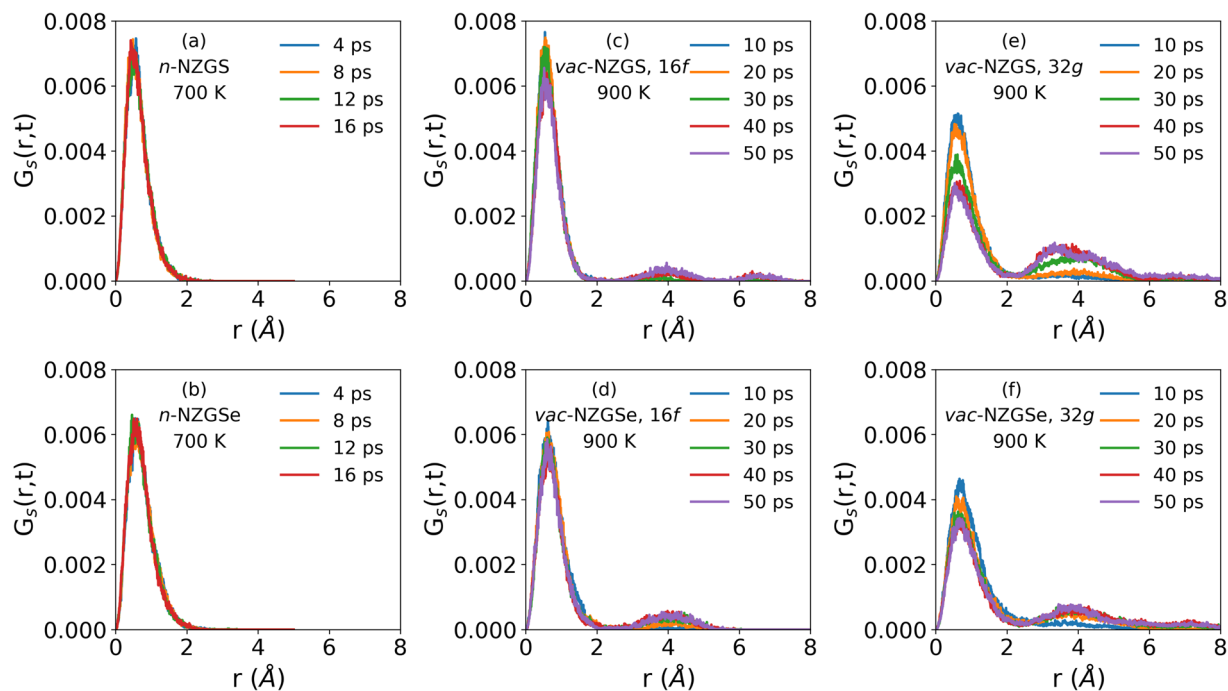
Fig. 7 (a and b) The calculated self Van–Hove correlation function, $G_s(r,t)$ of Na-ion of the stoichiometric compounds of Na_3ZnGaX_4 (X = S, Se) in the interval of 4 ps up to 20 ps at 700 K using AIMD. (c–f) The calculated Wyckoff site specific $G_s(r,t)$ of Na-ion in the 2% vacancy structure of Na_3ZnGaX_4 (X = S, Se) in the interval of 10 ps up to 50 ps at 900 K using AIMD.

AIMD (Fig. 7a and b), while for *vac*-NZGS and *vac*-NZGSe, we took up to 50 ps atomic trajectory with 10 ps intervals at 900 K as shown in Fig. S10.†(ref. 59) For *n*-NZGS and *n*-NZGSe, we didn't observe the evolution of any second or higher peak of Na ions, which means they just vibrate at the mean equilibrium position in each time frame. For *vac*-NZGS and *vac*-NZGSe, in the first 10 ps, the correlation function shows a single peak at ~ 0.8 Å, which means that the Na atoms are vibrating about equilibrium positions, and the area under the peak represents the number of Na$^+$. In the further time steps, the development of second peaks at ~ 4 Å with the reduction of intensities of the first peaks in the correlation function at discrete distances suggests a jump-like diffusion of Na$^+$ from one site to other sites with an average jump distance of around ~ 4 Å. The hopping rate is almost similar in both the Na-deficient chalcogenides compounds. To discriminate the hopping mechanism of Na atoms at 32*g* and 16*f* Wyckoff sites in each time frame, we calculated the Van–Hove correlation function separately for Na atoms at these sites (Fig. 7c–f). We found a significant change in the intensity and a rapid development of second and higher peaks of Na atoms at 32*g* sites in each time frame. This change provides a strong evidence that the Na atoms at 32*g* sites have a faster-hopping rate than the Na atoms at 16*f* sites.

We have calculated the pair distribution function, $g(r)$, for all pairs of atoms of both 2% Na vacancy chalcogenide compounds (*vac*-NZGS and *vac*-NZGSe) at various temperatures shown in Fig. S11a and S11b.†(ref. 59) The $g(r)$ of Na–Na pairs for *vac*-NZGS and *vac*-NZGSe shows the first neighbour Na distance at $\sim$4 Å in both compounds. The intensity of the first peak reduces with increasing temperature due to a larger thermal amplitude,

which further assists Na-diffusion. In contrast, the other pairs show negligible broadening with temperature, indicating these atoms vibrating at equilibrium positions and occupied in deep potential minima compared to Na sites. We have further calculated the Na–Na PDF for Na's at 32*g* and 16*f* Wyckoff sites for both compounds (*vac*-NZGS and *vac*-NZGSe) Fig. 5e and f. The Na at 16*f* sites shows sharper peaks than 32*g* Wyckoff sites, which shows that the Na in 32*g* has a shallower potential energy surface and predominantly participates in diffusion. Further, the sharpest $g(r)$ peak in Zn-X and Ga-X PDF at ~ 2 Å shows relatively rigid ZnX_4 and GaX_4 units, forming the host lattice.

5 Conclusions

We report the INS, QENS measurements and the AIMD simulations in both chalcogenide compounds Na_3ZnGaX_4 (X = S, Se). The INS result shows the presence of anharmonic phonons at elevated temperatures. Our AIMD simulations show the presence of low energy phonon modes of Na atoms at 32*g* Wyckoff sites in both compounds, which leads to Na hopping. The calculated harmonic phonon eigenvector of a typical low-E (~ 6 meV) phonon shows the large thermal amplitude of Na atoms at 32*g* sites for both compounds, which indicates a greater probability of leaving the sites. The QENS result shows significant quasielastic broadening at 700 K. The dependence of Lorentzian width with Q shows a long-range diffusion of the Na atom in both compounds. We found a similar magnitude of diffusion coefficient ($\sim 6 \times 10^{-10}$ m^2 s^{-1}) in both compounds. The calculated MSD in stoichiometric and 2% vacancy structure of Na_3ZnGaX_4 (X = S, Se) shows that vacancy is needed for Na

hopping. By calculating the Van–Hove self-correlation functions, we unravel that the Na atoms at 32g Wyckoff sites are more diffusive than the Na atoms at 16f sites. The calculated mean square displacement of individual Na atoms at 32g sites and 16f sites shows that many Na atoms hop in 30 ps while very few Na atoms hop through 16f sites.

We emphasize that it is important to identify the diffusion pathways, especially since the crystal structure offers different Na-sites (32g and 16f) and many different jump possibilities among these sites in three dimensions. The simulations have been extremely useful in identifying the diffusion pathways. We found that the diffusion occurs largely along certain zig-zag chain of the 32g sites. These chains are separated by $\sim c/4$ along the c-axis. We also observe jumps of Na ions from one chain to another along the c-axis. By computing the time-averaged Na-occupation probability, we have shown that Na-at 32g Wyckoff site are indeed connected through shallow energy landscape, providing the easy migration of Na-ions. In contrast, the energy landscape of the Na-16f Wyckoff sites involve large energy barriers and do not allow Na migration. Hence the presence of shallow energy landscape sites is essential for fast diffusion. Thus, despite the complex crystal structure, there exists certain topology of these chains that have a shallow potential and enable long-range diffusion. Existence and identification of such topologies is crucial for enhancing the Na-ion diffusion in Na$_3$ZnGaX$_4$ and other possible battery materials.

Conflicts of interest

There are no conflicts to declare.

Acknowledgements

References

1 A. Slameršak, G. Kallis and D. W. O'Neill, *Nat. Commun.*, 2022, **13**, 6932.

2 P. A. Owusu and S. Asumadu-Sarkodie, *Cogent Eng.*, 2016, **3**, 1167990.

3 D. Gielen, F. Boshell, D. Saygin, M. D. Bazilian, N. Wagner and R. Gorini, *Energy Strategy Rev.*, 2019, **24**, 38–50.

4 U. Bhattarai, T. Maraseni and A. Apan, *Sci. Total Environ.*, 2022, **833**, 155159.

5 V. P. Sharma, D. K. Somwanshi, K. Jain and R. K. Satankar, *IOP Conf. Ser.: Earth Environ.*, 2022, **1084**, 012002.

6 M. K. Gupta, J. Ding, D. Bansal, D. L. Abernathy, G. Ehlers, N. C. Osti, W. G. Zeier and O. Delaire, *Adv. Energy Mater.*, 2022, **12**, 2200596.

7 Q. Ren, M. K. Gupta, M. Jin, J. Ding, J. Wu, Z. Chen, S. Lin, O. Fabelo, J. A. Rodríguez-Velamazán, M. Kofu, K. Nakajima, M. Wolf, F. Zhu, J. Wang, Z. Cheng, G. Wang, X. Tong, Y. Pei, O. Delaire and J. Ma, *Nat. Mater.*, 2023, **22**, 999–1006.

8 T. M. Gür, *Energy Environ. Sci.*, 2018, **11**, 2696–2767.

9 S. Koohi-Fayegh and M. Rosen, *J. Energy Storage*, 2020, **27**, 101047.

10 T. Famprikis, P. Canepa, J. A. Dawson, M. S. Islam and C. Masquelier, *Nat. Mater.*, 2019, **18**, 1278–1291.

11 M. Armand and J. M. Tarascon, *Nature*, 2008, **451**, 652–657.

12 Q. Zhao, S. Stalin, C.-Z. Zhao and L. A. Archer, *Nat. Rev. Mater.*, 2020, **5**, 229–252.

13 A. Ponrouch, D. Monti, A. Boschin, B. Steen, P. Johansson and M. R. Palacín, *J. Mater. Chem. A*, 2015, **3**, 22–42.

14 J. M. Tarascon and M. Armand, *Nature*, 2001, **414**, 359–367.

15 J. Wang, L. Xu, G. Jia and J. Du, *Cryst. Growth Des.*, 2022, **22**, 5770–5784.

16 Y. Chen, Y. Kang, Y. Zhao, L. Wang, J. Liu, Y. Li, Z. Liang, X. He, X. Li, N. Tavajohi and B. Li, *J. Energy Chem.*, 2021, **59**, 83–99.

17 P. Yao, H. Yu, Z. Ding, Y. Liu, J. Lu, M. Lavorgna, J. Wu and X. Liu, *Front. Chem.*, 2019, **7**, 522.

18 N. Nitta, F. Wu, J. T. Lee and G. Yushin, *Mater. Today*, 2015, **18**, 252–264.

19 A. Sonoc and J. Jeswiet, *Procedia CIRP*, 2014, **15**, 289–293.

20 M. Hou, F. Liang, K. Chen, Y. Dai and D. Xue, *Nanotechnology*, 2020, **31**, 132003.

21 T. Ikeshoji, E. Tsuchida, T. Morishita, K. Ikeda, M. Matsuo, Y. Kawazoe and S.-i. Orimo, *Phys. Rev. B*, 2011, **83**, 144301.

22 N. Kamaya, K. Homma, Y. Yamakawa, M. Hirayama, R. Kanno, M. Yonemura, T. Kamiyama, Y. Kato, S. Hama, K. Kawamoto and A. Mitsui, *Nat. Mater.*, 2011, **10**, 682–686.

23 Y. Zhao and L. L. Daemen, *J. Am. Chem. Soc.*, 2012, **134**, 15042–15047.

24 R. Schlem, P. Till, M. Weiss, T. Krauskopf, S. P. Culver and W. G. Zeier, *Chem. - Eur. J.*, 2019, **25**, 4143–4148.

25 M. A. Kraft, S. P. Culver, M. Calderon, F. Böcher, T. Krauskopf, A. Senyshyn, C. Dietrich, A. Zevalkink, J. Janek and W. G. Zeier, *J. Am. Chem. Soc.*, 2017, **139**, 10909.

26 X. Lei, Y. Jee and K. Huang, *J. Mater. Chem. A*, 2015, **3**, 19920–19927.

27 M. K. Gupta, S. K. Mishra, R. Mittal, B. Singh, P. Goel, S. Mukhopadhyay, R. Shukla, S. N. Achary, A. K. Tyagi and S. L. Chaplot, *Phys. Rev. Mater.*, 2020, **4**, 045802.

28 Y. Sun, Y. Wang, X. Liang, Y. Xia, L. Peng, H. Jia, H. Li, L. Bai, J. Feng, H. Jiang and J. Xie, *J. Am. Chem. Soc.*, 2019, **141**, 5640–5644.

29 M. K. Gupta, J. Ding, N. C. Osti, D. L. Abernathy, W. Arnold, H. Wang, Z. Hood and O. Delaire, *Energy Environ. Sci.*, 2021, **14**, 6554–6563.

30 G. Sun, X. Yang, N. Chen, S. Yao, X. Wang, X. Jin, G. Chen, Y. Xie and F. Du, *Energy Stor. Mater.*, 2021, **41**, 196–202.

31 Z. Zhang, E. Ramos, F. Lalère, A. Assoud, K. Kaup, P. Hartman and L. F. Nazar, *Energy Environ. Sci.*, 2018, **11**, 87–93.

32 J. A. S. Oh, L. He, A. Plewa, M. Morita, Y. Zhao, T. Sakamoto, X. Song, W. Zhai, K. Zeng and L. Lu, *ACS Appl. Mater. Interfaces*, 2019, **11**, 40125–40133.

33 Q. Zhang, Q. Zhou, Y. Lu, Y. Shao, Y. Qi, X. Qi, G. Zhong, Y. Yang, L. Chen and Y.-S. Hu, *Engineering*, 2022, **8**, 170–180.

34 J. Schuett, F. Pescher and S. Neitzel-Grieshammer, *Phys. Chem. Chem. Phys.*, 2022, **24**, 22154–22167.

35 L. Gao, H. Zhang, Y. Wang, S. Li, R. Zhao, Y. Wang, S. Gao, L. He, H.-F. Song, R. Zou and Y. Zhao, *J. Mater. Chem. A*, 2020, **8**, 21265–21272.

36 J. A. Dawson, T. Famprikis and K. E. Johnston, *J. Mater. Chem. A*, 2021, **9**, 18746–18772.

37 H.-L. Yang, B.-W. Zhang, K. Konstantinov, Y.-X. Wang, H.-K. Liu and S.-X. Dou, *Adv. Energy Sustainability Res*, 2021, **2**, 2000057.

38 G. Deysher, Y.-T. Chen, B. Sayahpour, S. W.-H. Lin, S.-Y. Ham, P. Ridley, A. Cronk, E. A. Wu, D. H. S. Tan, J.-M. Doux, J. A. S. Oh, J. Jang, L. H. B. Nguyen and Y. S. Meng, *ACS Appl. Mater. Interfaces*, 2022, **14**, 47706–47715.

39 S. Takeuchi, K. Suzuki, M. Hirayama and R. Kanno, *J. Solid State Chem.*, 2018, **265**, 353–358.

40 S. Fujii, S. Gao, C. Tassel, T. Zhu, T. Broux, K. Okada, Y. Miyahara, A. Kuwabara and H. Kageyama, *J. Am. Chem. Soc.*, 2021, **143**, 10668–10675.

41 M. K. Gupta, S. Kumar, R. Mittal and S. L. Chaplot, *Phys. Rev. B*, 2022, **106**, 014311.

42 K. H. Park, D. H. Kim, H. Kwak, S. H. Jung, H.-J. Lee, A. Banerjee, J. H. Lee and Y. S. Jung, *J. Mater. Chem. A*, 2018, **6**, 17192–17200.

43 Y. Lu, L. Li, Q. Zhang, Y. Cai, Y. Ni and J. Chen, *Chem. Sci.*, 2022, **13**, 3416–3423.

44 M. Shimoda, M. Maegawa, S. Yoshida, H. Akamatsu, K. Hayashi, P. Gorai and S. Ohno, *Chem. Mater.*, 2022, **34**, 5634–5643.

45 S. Balijapelly, Q. Zhang, P. Sandineni, A. Adhikary, S. Mohapatra, S. Sundaramoorthy, N. Gerasimchuck, A. V. Chernatynskiy and A. Choudhury, *ACS Appl. Energy Mater.*, 2021, **4**, 7942–7951.

46 S. Han, J. Y. Seo, W. B. Park, A. B. Ikhe, S. Y. Choi, S. C. Han, K.-S. Sohn and M. Pyo, *J. Mater. Chem. A*, 2022, **10**, 25039–25046.

47 G. E. Granroth, A. I. Kolesnikov, T. E. Sherline, J. P. Clancy, K. A. Ross, J. P. C. Ruff, B. D. Gaulin and S. E. Nagler, *J. Phys.: Conf. Ser.*, 2010, **251**, 012058.

48 J. M. Carpenter and D. L. Price, *Phys. Rev. Lett.*, 1985, **54**, 441–443.

49 E. Mamontov and K. W. Herwig, *Rev. Sci. Instrum.*, 2011, **82**, 085109.

50 O. Arnold, J. C. Bilheux, J. M. Borreguero, A. Buts, S. I. Campbell, L. Chapon, M. Doucet, N. Draper, R. Ferraz Leal, M. A. Gigg, V. E. Lynch, A. Markvardsen, D. J. Mikkelson, R. L. Mikkelson, R. Miller, K. Palmen, P. Parker, G. Passos, T. G. Perring, P. F. Peterson, S. Ren, M. A. Reuter, A. T. Savici, J. W. Taylor, R. J. Taylor, R. Tolchenov, W. Zhou and J. Zikovsky, *Nuclear Instruments and Methods in Physics Research Section A: Accelerators, Spectrometers, Detectors and Associated Equipment*, 2014, **764**, 156–166.

51 G. Kresse and J. Furthmüller, *Phys. Rev. B*, 1996, **54**, 11169.

52 G. Kresse and J. Furthmüller, *Comput. Mater. Sci.*, 1996, **6**, 15–50.

53 J. Hafner, *J. Comput. Chem.*, 2008, **29**, 2044–2078.

54 G. Kresse and D. Joubert, *Phys. Rev. B*, 1999, **59**, 1758.

55 J. Perdew, K. Burke and M. Ernzerhof, *Phys. Rev. Lett.*, 1998, **80**, 891.

56 J. P. Perdew, K. Burke and M. Ernzerhof, *Phys. Rev. Lett.*, 1996, **77**, 3865.

57 A. Togo and I. Tanaka, *Scr. Mater.*, 2015, **108**, 1–5.

58 D. J. Evans and B. L. Holian, *J. Chem. Phys.*, 1985, **83**, 4069–4074.

59 See Supplementary Material for measured QENS data and calculated pair distribution functions , partial and total phonon DOS, MSD, and simulated S(Q,E) of Na3ZnGaX4 (X = S, Se). Various simulation details are also provided.

60 R. Chen, X. Wu and Z. Su, *Dalton Trans.*, 2018, **47**, 15538–15544.

61 C. T. Chudley and R. J. Elliott, *Proc. Phys. Soc.*, 1961, **77**, 353–361.